Analytical Chemistry, Volume 95, Issue 8, February 2023, pp. 4138-4146
DOI:10.1021/acs.analchem.2c05200

Entropy-driven three-dimensional DNA nano-fireworks for simultaneous real-time imaging of telomerase and microRNA in living cells

Jin Wang[1], Kaixuan Wang[1,3], Hanyong Peng[2], Zhen Zhang[1*], Zhugen Yang[3], Maoyong Song[2], Guibin Jiang[2]

[1]School of the Environment and Safety Engineering, Jiangsu University, Zhenjiang 212013, China.

[2]State Key Laboratory of Environmental Chemistry and Ecotoxicology, Research Center for Eco- Environmental Sciences, Chinese Academy of Sciences, Beijing 100085, China;

[3]School of Water, Energy, and Environment, Cranfield University, Cranfield MK43 0AL, UK;

ABSTRACT: Real-time monitoring of different types of intracellular tumor-related biomarkers is key importance for the identification of tumor cells. However, it is hampered by the low abundance of biomarkers, inefficient free diffusion of reactants, and complex cytoplasmic milieu. Herein, we present a stable and general method for in situ imaging of microRNA-21 and telomerase utilizing simple highly integrated dual tetrahedral DNA nanostructures (TDNs) that can naturally enter cells, which could initiate to form the three-dimensional higher-order DNA superstructures (DNA nano fireworks, DNFs) through a reliable target-triggered entropy-driven strand displacement reaction in living cells for remarkable signal amplification. Importantly, the excellent biostability, biocompatibility, and sensitivity of this approach benefited from (i) the precise multi-directional arrangement of probes with pure DNA structure, and (ii) the local target concentration enhanced by the spatially confined microdomain inside the DNFs. This strategy provides a pivotal molecular toolbox for a broad application such as biomedical imagine and early precise cancer diagnosis.

Keywords: Real-time monitoring, Signal amplification, Biosensor, Tetrahedral DNA nanostructure, Telomerase, MicroRNA

Introduction

The aberrant expression of some crucial cellular biomolecules is closely associated with tumor burden and malignant progression that could be used as biomarkers in early cancer diagnosis[1, 2]. Therein, telomerase, a kind of basic ribonucleoprotein reverse transcriptase that maintains continuous cell proliferation, is overexpressed in over 85% of human cancer cells but maintained at a very low level in normal cells[3]. In addition, abnormally upregulated expression of microRNA-21 (miRNA-21, a typical noncoding RNA) was found in most malignant tumors[4, 5]. Thus, simultaneous analysis of intracellular telomerase and miRNA-21 is important for accurate identification of tumor cells, which will avoid false-positives results relying on widely developed single target detection[6, 7]. However, this issue has not yet been well explored due to the low-abundance biomarkers and complex cytoplasmic environments[8, 9]. Furthermore, conventional analytical methods based on cell extracts cannot provide real-time information related to intracellular biological dysfunction and tumor progression[10, 11]. To this end, an in-situ method with high stability and acceptable accuracy is in great demand for visualization of telomerase and miRNA-21 in living cells.

DNA nanotechnology recently opens up huge opportunities for monitoring target molecules in the complex cellular milieu owing to its high biocompatibility, programmability, and controllability[12, 13]. Albeit important, grand challenges still remain at many aspects of DNA nanostructure-based methods[14]: (i) the weak biostability of complicated probes using nucleic acid nanostructures make them difficult to resist poor cell permeation and fragility in complex cytoplasmic milieu[15, 16]; (ii) enzyme-based DNA reactions are often accompanied by changes in the number of base pairs, which reduces the reliability of output results[17, 18]; (iii) most DNA nanostructure-based probes are inefficient due to single orientation and lack of spatially confined arrangement[19, 20]; (iv) the complex architectures using nucleic acid reagents or nonbiological nanomaterials suffer from their insufficient delivery into cells and potential toxicity because of heterogeneity in composition and surface chemistry[21, 22]. These drawbacks call for a rationally designed DNA nanoarchitecture which possess sufficient biocompatibility and easy to assemble, while maintaining accurate probe arrangement and high stability in living cells[23].

Tetrahedral DNA nanostructures (TDNs), as a robust small-scale three-dimensional (3D) framework[24, 25], will improve its enzyme resistance and natural biocompatibility with negligible toxicity[26, 27]. Besides, the design of its unique spatial structure provides an excellent carrier for the precise arrangement of probes in multiple directions[28, 29]. Signal amplification approaches based on TDNs were considered as effective tools for sensitive detection of targets owing to their high reliability[30]. However, traditional hairpin-based amplification strategies using TDN monomers as carriers, like catalytic hairpin assembly (CHA) and hybridization chain reaction (HCR), are constricted by relatively high background and false-positive results[31], implying some hindrances for the application in living cells[32]. In contrast, entropy-driven strand displacement reaction occurs in a catalytic circuit through toehold-assisted branch migration[33], provides a possibility for in situ quantification of intracellular targets by means of a simple enzyme-free DNA amplifier. The reaction is driven by entropy increase without being changed of the total number of base pairs, therefore this signal amplification strategy can effectively reduce the potential circuit leakage and significantly improves the robustness of self-sustained reaction in complex cytoplasmic milieu[34, 35].

Herein, a TDNs-based entropy-driven signal amplification strategy was proposed using synthesized simple dual TDNs probes for simultaneous visualization of intracellular miRNA and telomerase in real-time. Owing to their small size and unique architecture constructed by pure DNA nanomaterials, TDNs probes could achieve cellular self-delivery through endocytosis without the help of transfection agents[36], and displayed almost nontoxic and highly biocompatible[37, 38]. The formation of 3D superstructures for cell imaging through intracellular self-assembly triggered by entropy-driven strand displacement reaction looks like dazzling fireworks, named by the "DNA nano fireworks" (DNFs), indicating excellent sensitivity, significant biostability, and reliability, which was put forward by entropy increase instead of free-energy released from base pairs generation, and showed more reliable and accurate than that using HCR and CHA[32]. Furthermore, according to reactive collision theory, multidirectional probes based on a spatially

Published by American Chemical Society. This is the Author Accepted Manuscript issued with: Creative Commons Attribution Non-Commercial License (CC:BY:NC 4.0).
The final published version (version of record) is available online at DOI:10.1021/acs.analchem.2c05200. Please refer to any applicable publisher terms of use.

confined arrangement inside DNFs, increased the local concentration and collision probability of reactants. Ascribed to these advantages, the DNFs-based signal amplification strategy tremendously reduced various interferences from nuclease and other substances in living cells. Through parameter verification and systematic investigation, this method has been successfully applied for imaging intracellular miRNA-21 and telomerase, showing to be an effective tool in the discrimination of non-tumorigenic and malignant tumor cells.

EXPERIMENTAL METHODS

Fluorescence experiments in vitro. For the fluorescence response of miRNA, different concentrations miRNA single nucleotide sequences were added into the Tris-HCl buffer solution (25 mM Tris with 5 mM $MgCl_2$, pH=8.0) containing 25 nM each of P and A-TDNs at 37 °C for 60 min. Similarly, we verified the ability of the proposed TDN probes to detect telomerase. 1 mM dNTPs with cell extract containing different concentrations of telomerase were added to the solution and reacted at 37 °C for 60 min, then heated to 95 °C for 15 min to inactivate telomerase. The resulting mixture was directly used for fluorescence determination without further treatment. For fluorescence intensity scan, the excitation (Ex) wavelength for Cy3 is 530 nm, and measured from 550 to 650 nm in 1 nm increment and the excitation (Ex) wavelength for Cy5 is 635 nm, and measured from 655 to 710 nm in 1 nm increment. All experiments were repeated at least three times.

Confocal fluorescence imaging. For confocal imaging studies, HeLa, HepG2, MCF-7, MCF-10A, and MRC-5 cells were cultured in 35-mm confocal laser culture dishes for 24 h with 5% O_2. After washed three times by PBS solution, the cells were pretreated with 1 mL medium containing 100 nM of P and A-TDNs for 6 h. Then, the cells were washed three times again using PBS solution, 1 mL of medium (without phenol red) was added for fluorescence imaging. All the imaging pictures of the cells were acquired using a Leica TCS SP5 II Laser confocal laser scanning microscopy (CLSM, Leica Microsystems, Inc., Wetzlar, Germany) with a 40× objective. Fluorescence signal of Cy3 was measured by sequential excitation at 535 nm and collected over 550-650 nm; Cy5 was obtained by excitation at 635 nm and measured over 655-710 nm.

RESULTS AND DISCUSSION

Assembly and working principle of TDN probes. As shown in Scheme 1 and Table S1, two kinds of TDNs (probe TDNs, P-TDNs; auxiliary TDNs, A-TDNs) were built using a set of T17 DNA backbone sequences with the size of 10 nm (displayed in Figure 1a and b), where four extended cantilevers at the vertices of the tetrahedral framework were arranged as the specific probes against two targets (P-TDNs) or the fuel strands assisted in signals amplification (A-TDNs), which will be completely quenched by high-efficiency of Black Hole Quencher (BHQ-2) owing to the special locked sequences of the modules before their cellular uptake, and they will maintain the monodispersed state in the absence of targets.

When the quenched P-TDNs were transported into the cells by endocytosis, displayed by Scheme 1, the intracellular miRNA-21 would bind to the single-stranded probes (P1 and P2), resulting in the shedding of the complementary short strand with the quencher (P5) and the exposure of a domain on the probes. At the same time, the telomerase primer (TP) sequence will extend as repeated 5'-TTAGGG-3' DNA segments to be continuously added onto the 3' end, and P6/TP double-stranded DNA (dsDNA) structures will be completed by elongated sequence on the TP region and fall off from the P-TDN monomers, causing the entire domain exposed on the extended cantilevers of P3 and P4. Consequently, auxiliary sequences (A1-4) on the A-TDNs promptly connect the exposed domain of P-TDNs by entropy-driven strand displacement reaction, triggering a 3D DNFs through intracellular self-assembly with "hand in hand" formation, along with significantly enhanced fluorescent signals for sensitive cell imaging due to the increase of local probes concentration and orderly arrangement of Cy3/Cy5 fluorescent dyes inside the 3D space architecture, and the fluorescent intensity is closely related to intracellular biomarkers levels.

Characterization of DNA nanostructures. The successful formation of TDNs and DNFs was authenticated by 2% agarose gel electrophoresis. Seen in Figure. 1a (I) and (II), the migration speed of the electrophoretic bands decreased significantly after the gradual addition of oligonucleotide strands, and the slowest migration was observed in lane 5, demonstrating the successful preparation of TDNs. In addition, as shown in Figure. 1a (III), TDN monomers (lane 6) maintained their monodisperses in a mixed solution containing two types of TDNs loaded with short strands (quenchers, P5, P6, A5, and A6). Additionally, according to our design, the macromolecular 3D DNA nano-superstructures (DNFs) were formed after the efficient combination of two TDNs in the absence of short strands (modified with quenchers), implying an outstanding blocking effect of well-designed short strands and a high binding efficiency of cantilevers between TDN modules (lane 5). Meanwhile, atomic force microscope (AFM) and dynamic light scattering (DLS) were used for further confirmation of corresponding DNA final products (two TDNs and DNFs). In Figure 1b, the monomeric TDNs showed bright dots with good monodisperses (Group I and II) due to their small size (17-bp side length). By comparison, DNF superstructures present irregular shape with a diameter of more than 300 nm (Figure 1b Group III). Moreover, as illustrated in Figure S1, the results of dynamic light scattering (DLS) are consistent with the characterization by AFM. All of the above data demonstrated that TDNs and DNFs were well prepared according to our pre-planned rational design.

Given that both two TDN probes were key factors to fabricate DNFs, their reliability was estimated by the fluorescent response of short strands on the cantilevers of TDNs with or without quencher modification, and the fluorescence intensity of Cy3/Cy5 represents the levels of two targets. Figure S2 indicated that the absolute quenching of fluorophores with negligible fluorescence background appeared after quenching sequences hybridized with corresponding sequences on the cantilevers of TDN monomers. In contrast, strong fluorescence was observed in the absence of quenching consequence, signifying that the fluorescent nanoprobes were successfully prepared and feasible for the presence of the biomarkers. In addition, according to our design, as a key step of the entropy-driven strand displacement system, the quencher-free P-TDNs should be able to trigger the connection with the A-TDNs via hybridization of the cantilever sequences, which was verified by the results in Figure 1c and d. When both quencher-free P-TDNs and A-TDNs exist in this system, a strong fluorescence signal appeared, further confirming the successful fabrication of DNFs.

Evaluation of the in vitro sensing performance. The sensitivity of the constructed sensing platform was estimated after the addition of the solutions containing different concentrations of both targets. As illustrated by Figure 2a and b, a dynamic correlation between the Cy3 fluorescent signal and the concentration of miRNA-21 was observed in the range of 0-2000 pM. Calculated based on the 3σ method (Group I in Figure 2a and

b), the limit of detection (LOD) of this method is 34 pM[39, 40]. Compared to the reported strategies with fluorescence analysis based on nucleic acid nanomaterials (displayed in Table S2), our proposed DNFs showed a higher sensitivity for this target detection. Similarly, the Cy5 fluorescence intensity proportionally increased with varying concentrations of HeLa cell extracts (containing the corresponding level of telomerase) ranging from 0 to 1.6×10^4 cells/μL (Group II in Figure 2a and b), and LOD is calculated as 100 cells/μL according to the average signal of three times of standard deviation of the control[41, 42], showing a comparative sensitivity with the previous methods (Table S3). All the above results demonstrated that our proposed DNFs can sensitively detect both targets at low abundance. On the other hand, fluorescence kinetic experience confirmed the high sensitivity and efficiency of the P/A-TDNs synergic system (Figure S3).

In addition, the selectivity of proposed nanoprobes for the respective response of miRNA-21 and telomerase was also investigated since that is a key parameter for this method. As seen in Figure 2c, after adding single-base mismatched miRNA-21 (SM miRNA-21), three-base mismatched miRNA-21 (TM miRNA-21), miRNA-155, miRNA-210, and miRNA-221 to the detection system, respectively, only miRNA-21 with correct sequence could initiate a significant Cy3 fluorescence. For comparison, the caused fluorescence signals by all other variants were negligible (around the baseline level), indicating the outstanding specificity of this sensing platform against miRNA-21. Besides, in the selectivity evaluation of telomerase, bovine serum albumin (BSA), Bst DNA polymerase (Bst), untreated and heated HeLa cell extracts (from 5000 cells) were classified as controls, and untreated HeLa cell extracts containing active telomerase were used as the test Group. Figure 2d showed that strong Cy5 fluorescence was observed only in the test Group, meaning that the detection system possesses good specificity for telomerase, which was also supported by further agarose gel electrophoresis. As shown in Figure S4, different from the single band of individual TP (Lane 1), TP that was incubated with HeLa cell extracts exhibited elongated bands (Lane 3), implying that the repeated 5'-TTAGGG-3' DNA segments could be continuously collected to 3' end of TP by telomerase. To further verify the selectivity of DNFs against telomerase, a proof-of-concept assay was performed after respectively adding five cell lines extracts (HeLa, HepG2, MCF-7, MCF-10A, and HK-2) into test solution containing DNA nanoprobes to discriminate non-tumorigenic and malignant tumor cells. Figure 2e illustrated that intense Cy5 fluorescence was generated only in tumor cell extracts, on the contrary, signal around baseline was observed in non-tumor cell lines (MCF-10A and HK-2), demonstrating the excellent specificity of DNFs for telomerase. Meanwhile, one interesting finding is that the telomerase activity is relatively high in HeLa cells while relatively low in MCF-7 and HepG2 cells, which is consistent with previous literatures[42]. The results of the sensitivity and selectivity assessments revealed that the constructed TDN nanoprobes could be applied as a sensitive and specific DNA amplifier to identify tumor cells and non-tumor cells using telomerase and miRNA-21 as cancer biomarkers.

Furthermore, the fabricated TDN probes and a qRT-PCR experiment (using commercial kits) were applied for analysis of miRNA-21 in five different cell line extracts. Seen in Table S4, there was a good correlation between the two methods, implying the reliability of our method for the detection of miRNA-21. In addition, shown as Figure S5, after calibrated telomerase levels from different Hela cell extracts with enzyme-linked immunosorbent assay (based on commercial kits), our method was evaluated by a spike-recovery experiment using 1% FBS containing Hela cell extracts with different concentration of telomerase, and the result (Table S5) exhibited that fabricated TDN probes are reliable for telomerase analysis depending on its satisfactory accuracy (recoveries, 91.6- 115.3%; RSD, 3.5-6.4%). All the above assessments demonstrated our method could be used in real samples or simulated biological samples.

Biostability, cellular cytotoxicity, and uptake study of DNFs. To investigate the biostability of DNFs responding to intrinsic interferences caused by enzymatic digestion and side effects by varied pH conditions inside cytoplasmic milieus, which will bring about potential false-positive signals, two commonly existed conditions including 10% FBS and 0.5 U/mL DNase I were incubated with DNFs for 8 hours, respectively, and the final products were confirmed by agarose gel electrophoresis. Figure S6a showed that negligible fluorescence intensity changes were observed after continuous incubation, and the bands at the same positions implied that their structural integrity remained unaltered (Figure S6b). In addition, the tolerance of DNFs under different pH conditions was investigated in the range of pH 5-9. As shown in Figure S6c, DNFs displayed satisfactory resistance at different pH values, and Figure S6d demonstrated that the macromolecular morphology of DNFs was not altered. These results indicate that the DNFs have prominent adaptability for complex cellular milieu and excellent pH tolerance. The prominent biological stability of the proposed DNFs is derived from the steric hindrance and structural rigidity of its DNA monomer framework structures (TDNs), which provided an important precondition for subsequent studies in living cells.

HeLa cells were used as a model to evaluate the cytotoxicity and cellular uptake of the nanoprobe in living cells. Firstly, Cell Counting Kit-8 (CCK-8) was implemented for cell viability assessment after co-incubation with DNFs. As shown in Figure S7, cells retained over 86.2% viability after the treatment of DNFs, even though 48 hours of incubation and the concentration up to 200 nM, indicating its excellent biocompatibility, ascribed to its unique structure made up of pure DNA nanomaterials[43, 44]. These results suggested that the TDN nanoprobes did not cause obvious damage to cells throughout the intracellular reaction and can be applied to living cell imaging.

At the same time, cellular uptake was tested using confocal laser scanning microscopy (CLSM) after HeLa cells were respectively incubated with 100 nM P and A-TDNs under a certain time (0, 4, 8, and 16 hours). As shown in Figure S8a, preliminary fluorescence was observed after the incubation for 4 hours. Subsequently, a bright fluorescence appeared at the incubation time of 8 hours, and this fluorescent intensity could remain stable for at least 16 hours. Furthermore, fluorescence intensity-time variations in living cells were confirmed by the calculation of the fluorescence profile of the designated region (Figure S8b). Then, we used five different cell lines (Hela, HepG2, MCF-7, MCF-10A, MCR-5) to verify the cellular uptake efficiency of TDN probes. As shown in Figure S9, after incubated with 100 nM TDNs (without quencher) for 8 h, all cell lines showed significant Cy3/Cy5 fluorescence signals, suggesting that most TDN monomers have been absorbed by living cells. The above findings suggest that our proposed TDN nanoprobes have high membrane permeability and can enter living cells without the help of transfection agents due to their structural rigidity[45, 19].

Bioimaging for living cells. The capability of established nanoprobes was systematically investigated for in situ imaging of tumor-related miRNA-21 and telomerase in living cells, the real-time levels of which could reflect the cancer progress, and fluorescence signals were recorded by CLSM[46-48]. In addition, TDN fluorescent probes were applied in Hela cells to evaluate their ability to dynamically visualize the changes of specific intracellular targets. Firstly, to demonstrate that the observed Cy3 fluorescence signal was indeed related to the expression levels of miRNA-21 in living cells, miRNA-21 inhibitor/mimic was designed to treat Hela cells for downregulation/ upregulation of miRNA expression, respectively (Figure 3a), and non-treated Hela cells were used as controls. Hela cells treated with miRNA-21 mimic showed stronger Cy3 fluorescence (III) compared to the control Group (II). On the contrary, almost no fluorescence was observed in Group I, representing negligible miRNA-21 was detected in Group I. All of these demonstrate that the TDN nanoprobes can sensitively visualize different expression levels of miRNA-21 in living cells. Likewise, to verify the ability of the nanoprobes for sensitive imaging of telomerase activity and to further validate that telomerase triggered the Cy5 fluorescence restoration in living cells, HeLa cells with diverse concentrations of telomerase activity were pre-treated with three concentrations (60, 120, and 240 μg/mL) of epigallocatechin gallate (EGCG, a well-characterized telomerase inhibitor). As shown in Figure S10a, the fluorescence intensity of Cy5 gradually decreased with the increase of EGCG, which correlated with the decrease of telomerase activity. Moreover, ImageJ software was used to analyze the fluorescence profiles of the middle cross-section in living cells, which showed a consistent Cy3/Cy5 signal change trend (Figure 3b and S10b), implying that the developed nanoprobes held the potential for highly sensitive miRNA-21 and telomerase detection. In addition, we noticed that the fluorescence intensity of Cy3/Cy5 can change individually with the corresponding target level, suggesting that the TDN nanoprobes can independently image a single target in situ and avoid the mutual interference of two fluorescent signals.

Meanwhile, three cancer cell lines (Hela, HepG2, MCF-7) and two control cell lines (MCF-10A, MCR-5) were selected to verify the practical applicability of the proposed nanoprobes in accurately identifying non-tumorigenic and malignant tumor cells, and the Cy3/Cy5 fluorescence signals from living cells were presented by CLSM. As shown in Figure 4a, three cancer cell lines (HeLa, HepG2, and MCF-7) simultaneously displayed two significant fluorescence (Cy3 fluorescence corresponding to miRNA-21 and Cy5 fluorescence referring to telomerase, respectively). In contrast, almost no Cy3 or Cy5 fluorescence was observed in normal cell lines (MCF-10A and MRC-5). Furthermore, Cy3/Cy5 fluorescence intensity analysis along the yellow line is in accordance with the outputs from CLSM (Figure 4b) and reflected that not only are TDN nanoprobes easily internalized but also they can respond to both targets in living cells, which is perfectly consistent with the qRT-PCR results (Table S4) and previous reports[49, 50]. These results demonstrate the reliability of the constructed method for discriminating normal cells from tumor cells based on miRNA-21 and telomerase as biomarkers.

CONCLUSIONS

In summary, a dual TDN nanoprobes system with excellent biostability and biocompatibility were developed, which can achieve cellular self-delivery through endocytosis. After triggered by miRNA-21 and telomerase in living cells, it rapidly forms an enlarged 3D DNA framework (DNFs) by intracellular self-assembly with significantly enhanced fluorescence for simultaneously sensitive imaging of the two targets. Besides, integrating the advantages of a rational spatially confined arrangement and a precise entropy-driven enzyme-free strand displacement design, our sensing platform demonstrated its reliability in accurately discriminate the non-tumorigenic and malignant tumor cells in real-time. Therefore, we believe that our strategy has clear potential for early diagnosis of cancer and other diseases.

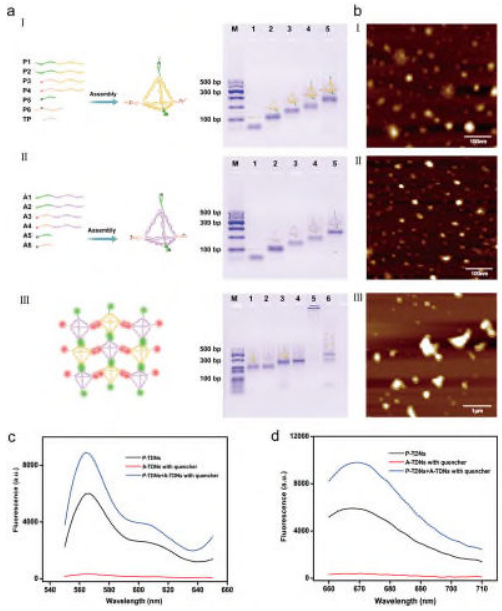

Figure 1. Characterizations of the TDNs and 3D DNFs. a Feasibility tests of TDNs and DNFs preparation process using agarose gel analysis. The self-assembly of TDNs is performed individually. Groups I and II respectively show the step-by-step preparation process of the P and A-types TDNs. The concentration of the TDNs was 1 μM. Group III shows the successful assembly of 3D DNA nano fireworks with two TDNs as units. DNA marker, 100 bp ladder from 25 to 500 bp. b AFM images of FNAs products of each Group in a. Groups I and II show the monomeric P and A-types TDNs. Group III shows the 3D DNA nano fireworks generated by two TDNs. c, d Fluorescence spectral responses of the P and A-types TDNs. The concentration of the TDNs was 100 nM (c and d are the fluorescence of Cy3 at 570 nm and of Cy5 at 670 nm, respectively).

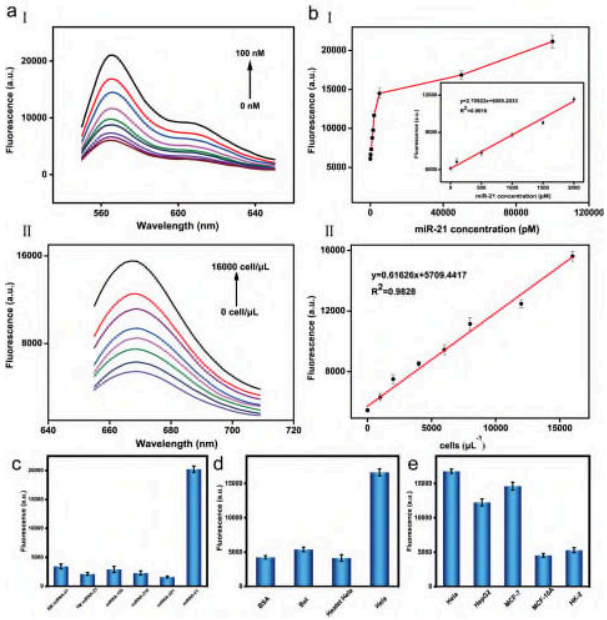

Figure 2. a Groups I: fluorescence spectral changes of the sensing system in the presence of different concentrations of miRNA-21, ranging from 0 to 100 nM. Groups II: fluorescence spectral changes of the sensing system with telomerase extracts come from different amounts of HeLa cells. b Groups I: miRNA-21 concentration-dependent changes in the fluorescence of Cy3. Inset: the linear relationship between the fluorescence intensity and the miRNA-21 concentration in the range of 0-2000 pM. Groups II: The relationship between the fluorescence intensity and different concentrations of HeLa cell extracts. c Fluorescence response of the sensing system to SM miR-21, TM miR-21, miR-155, miR-210, and miR-221, respectively. Concentration of all the miRNAs is 100 nM. d Fluorescence response of the sensing system to telomerase extracted from BSA, Bst, extracts, and heated extracts from 15000 HeLa cells, respectively. e Telomerase activity detection for various cell lines. The concentrations of all tested cells are 15000 cells/μL.

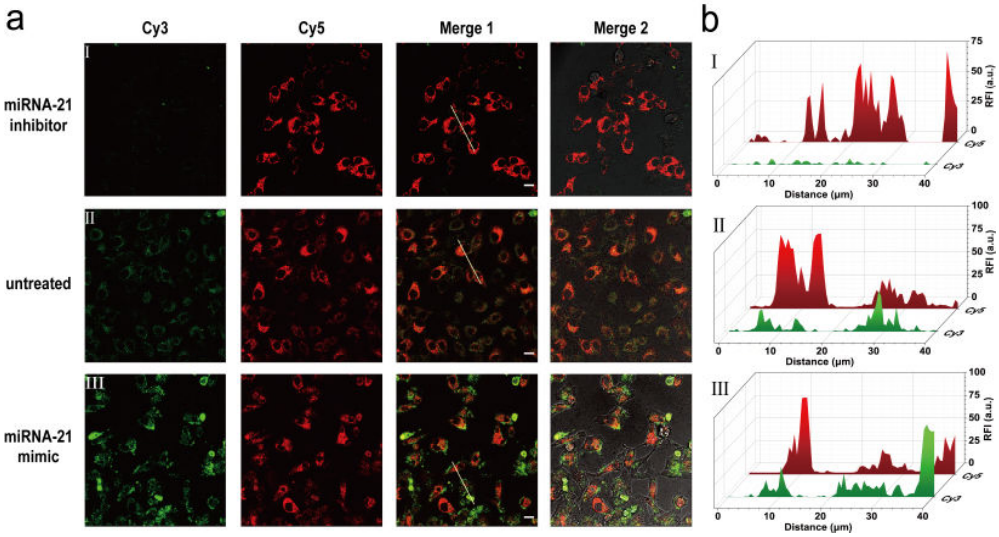

Figure 3. a CLSM images of miRNA-21 in untreated HeLa cells (II), miRNA-21 inhibitor (I) and mimic (III)-transfected HeLa cells. HeLa cells were incubated with 100 nM TDNs for 8 h at 37 ℃. Scale bars, 10 μm. Merge 2 contains the overlap of bright-field. b Cy3 and Cy5 fluorescence intensity of the linear regions of each Group in a. Groups I, II, and III, respectively, represent the independent Groups in a from top to bottom. RFI: relative fluorescence intensity.

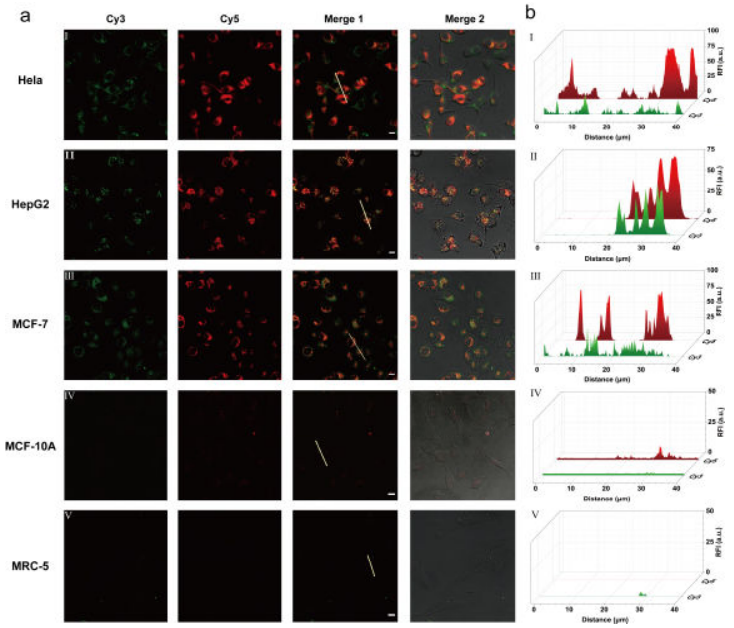

Figure 4. a CLSM images of HeLa (I), HepG2 (II), MCF-7 (III), MCF-10A (IV), MCR-5 (V) cells incubated with 100 nM TDNs for 8 h at 37 ℃. Scale bars, 10 μm. Merge 2 contains the overlap of bright-field. b Cy3 and Cy5 fluorescence intensity of the linear regions of each Group in a. Groups I, II, III, IV, and V, respectively, represent the independent Groups in a from top to bottom. RFI: relative fluorescence intensity.

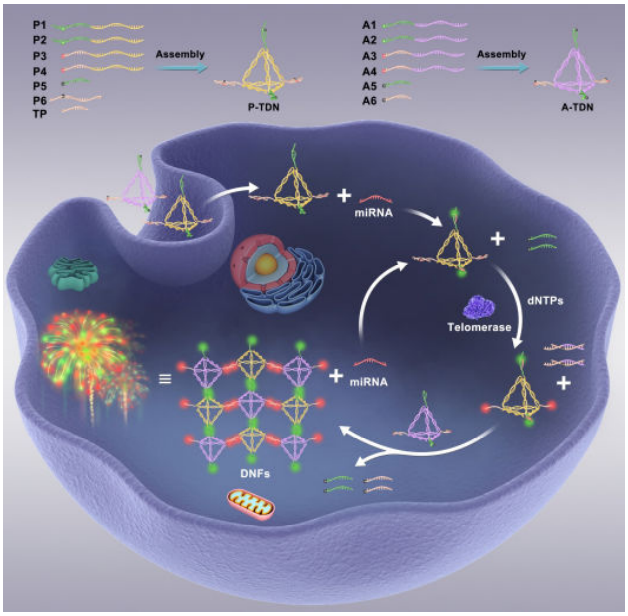

Scheme 1. Schematic illustrations of 3D DNA nano-fireworks for the simultaneous real-time imaging of telomerase and miRNA in living cells. The two monomeric TDNs are taken up by the cells and triggered by dual targets to form 3D DNA nano-fireworks.

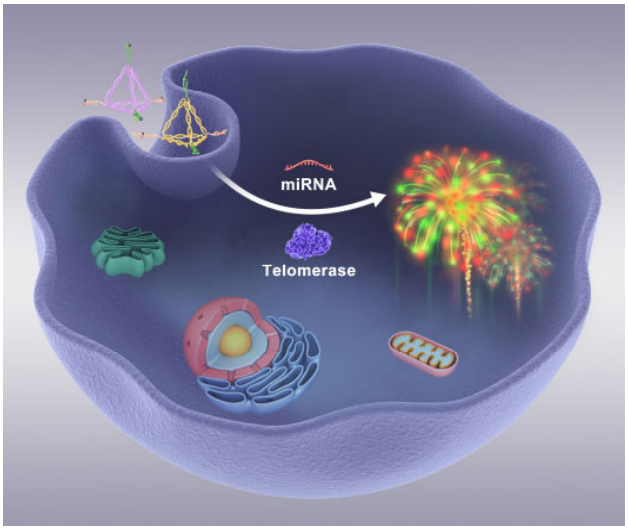

Graphical Abstract

ASSOCIATED CONTENT

Supporting Information

The Supporting Information is available free of charge on the ACS Publications website.

Chemicals and materials; cell culture; apparatus; Sequences; data analysis; cytotoxicity study; and cell fluorescence imaging (PDF)

AUTHOR INFORMATION

Corresponding Author

Zhen Zhang- School of the Environment and Safety Engineering, Jiangsu University, Zhenjiang 212013, China
Email: zhangzhen@ujs.edu.cn

Authors

Jin Wang- School of the Environment and Safety Engineering, Jiangsu University, Zhenjiang 212013, China
Email: jinwang_ujs@163.com

Kaixuan Wang- School of the Environment and Safety Engineering, Jiangsu University, Zhenjiang 212013, China; School of Water, Energy, and Environment, Cranfield University, Cranfield MK43 0AL, UK
Email: heer08@126.com

Hanyong Peng- State Key Laboratory of Environmental Chemistry and Ecotoxicology, Research Center for Eco- Environmental Sciences, Chinese Academy of Sciences, Beijing 100085, China
Email: hypeng@rcees.ac.cn

Zhugen Yang- School of Water, Energy, and Environment, Cranfield University, Cranfield MK43 0AL, UK
Email: zhugen.yang@cranfield.ac.uk

Maoyong Song- State Key Laboratory of Environmental Chemistry and Ecotoxicology, Research Center for Eco- Environmental Sciences, Chinese Academy of Sciences, Beijing 100085, China
Email: mysong@rcees.ac.cn

Guibin Jiang- State Key Laboratory of Environmental Chemistry and Ecotoxicology, Research Center for Eco- Environmental Sciences, Chinese Academy of Sciences, Beijing 100085, China
Email: gbjiang@rcees.ac.cn

Author Contributions

All authors have given approval to the final version of the manuscript.

Notes

The authors declare no competing financial interest.

ACKNOWLEDGMENT

The present work was supported by the National Natural Science Foundation of China (Grants 21876067, 21577051), and Jiangsu Collaborative Innovation Center of Technology and Material of Water Treatment. In addition, we specially want to thank Professor Yi Lu and his team at the department of Chemistry, University of Texas, Austin for expert advice and fruitful discussions.

REFERENCE

(1) Yang, Y.; Zeng, B.; Li, Y.; Liang, H.; Yang, Y.; Yuan, Q., *Science China Chemistry* **2020,** *63* (7), 997-1003.
(2) Yang, Q.; Yang, F.; Dai, W.; Meng, X.; Wei, W.; Cheng, Y.; Dong, J.; Lu, H.; Dong, H., *Adv Healthc Mater* **2021,** *10* (21), e2101130.
(3) Ma, Y.; Wang, Z.; Zhang, M.; Han, Z.; Chen, D.; Zhu, Q.; Gao, W.; Qian, Z.; Gu, Y., *Angewandte Chemie International Edition* **2016,** *55* (10), 3304-3308.
(4) Bhome, R.; Del Vecchio, F.; Lee, G.-H.; Bullock, M. D.; Primrose, J. N.; Sayan, A. E.; Mirnezami, A. H., *Cancer Letters* **2018,** *420*, 228-235.
(5) Agbu, P.; Carthew, R. W., *Nature Reviews Molecular Cell Biology* **2021,** *22* (6), 425-438.
(6) Eckburg, A.; Dein, J.; Berei, J.; Schrank, Z.; Puri, N., *Cancers (Basel)* **2020,** *12* (9).
(7) Guo, X.; Wu, X.; Sun, M.; Xu, L.; Kuang, H.; Xu, C., *Anal Chem* **2020,** *92* (2), 2310-2315.
(8) Ou, X.; Zhan, S.; Sun, C.; Cheng, Y.; Wang, X.; Liu, B.; Zhai, T.; Lou, X.; Xia, F., *Biosensors and Bioelectronics* **2019,** *124-125*, 199-204.
(9) Xue, J.; Chen, F.; Bai, M.; Cao, X.; Huang, P.; Zhao, Y., *Analytical Chemistry* **2019,** *91* (7), 4696-4701.
(10) Huang, Q.; Ma, P.-Q.; Li, H.-D.; Yin, B.-C.; Ye, B.-C., *ACS Applied Bio Materials* **2020,** *3* (5), 2861-2866.
(11) Wang, H.; Peng, P.; Wang, Q.; Du, Y.; Tian, Z.; Li, T., *Angewandte Chemie International Edition* **2020,** *59* (15), 6099-6107.
(12) Peng, P.; Du, Y.; Zheng, J.; Wang, H.; Li, T., *Angewandte Chemie International Edition* **2019,** *58* (6), 1648-1653.
(13) Shi, J.; Shen, M.; Zhao, W.; Liu, J.; Qu, Z.; Zhu, M.; Chen, Z.; Shi, P.; Zhang, Z.; Zhang, S.-S., *ACS Applied Materials & Interfaces* **2021,** *13* (43), 51393-51402.
(14) Gao, T.; Chen, T.; Feng, C.; He, X.; Mu, C.; Anzai, J.-i.; Li, G., *Nature Communications* **2019,** *10* (1), 2946.
(15) Wei, Q.; Huang, J.; Li, J.; Wang, J.; Yang, X.; Liu, J.; Wang, K., *Chemical Science* **2018,** *9* (40), 7802-7808.
(16) Wu, H.; Chen, T.-T.; Wang, X.-N.; Ke, Y.; Jiang, J.-H., *Chemical Science* **2020,** *11* (1), 62-69.
(17) Zhang David, Y.; Turberfield Andrew, J.; Yurke, B.; Winfree, E., *Science* **2007,** *318* (5853), 1121-1125.
(18) Wang, J. S.; Yan, Y. H.; Zhang, D. Y., *Nature Chemistry* **2017,** *9* (12), 1222-1228.
(19) Wang, D. X.; Wang, J.; Cui, Y. X.; Wang, Y. X.; Tang, A. N.; Kong, D. M., *Anal Chem* **2019,** *91* (20), 13165-13173.
(20) Gong, X.; He, S.; Li, R.; Chen, Y.; Tan, K.; Wan, Y.; Liu, X.; Wang, F., *Chemical Science* **2022,** *13* (35), 10428-10436.
(21) Li, S.; Tian, T.; Zhang, T.; Cai, X.; Lin, Y., *Materials Today* **2019,** *24*, 57-68.
(22) Li, C.; Luo, S.; Wang, J.; Shen, Z.; Wu, Z. S., *Nanoscale* **2021,** *13* (15), 7034-7051.
(23) Xue, C.; Zhang, S.; Yu, X.; Hu, S.; Lu, Y.; Wu, Z.-S., *Angewandte Chemie International Edition* **2020,** *59* (40), 17540-17547.
(24) Li, C. H.; Lv, W. Y.; Yang, F. F.; Zhen, S. J.; Huang, C. Z., *ACS Applied Materials & Interfaces* **2022,** *14* (10), 12059-12067.
(25) Zhang, B.; Tian, T.; Xiao, D.; Gao, S.; Cai, X.; Lin, Y., *Advanced Functional Materials* **2022**, 2109728.
(26) Zhang, J.; Guo, Y.; Ding, F.; Pan, G.; Zhu, X.; Zhang, C., *Angewandte Chemie* **2019,** *58* (39), 13794-13798.
(27) Li, F.; Liu, Y.; Dong, Y.; Chu, Y.; Song, N.; Yang, D., *J Am Chem Soc* **2022,** *144* (10), 4667-4677.
(28) Frtus, A.; Smolkova, B.; Uzhytchak, M.; Lunova, M.; Jirsa, M.; Henry, S. J. W.; Dejneka, A.; Stephanopoulos, N.; Lunov, O., *Acta biomaterialia* **2022,** *146*, 10-22.
(29) Li, S.; Liu, Y.; Zhang, T.; Lin, S.; Shi, S.; He, J.; Xie, Y.; Cai, X.; Tian, T.; Lin, Y., *Adv Mater* **2022,** *34* (46), e2204287.
(30) Shi, S.; Li, Y.; Zhang, T.; Xiao, D.; Tian, T.; Chen, T.; Zhang, Y.; Li, X.; Lin, Y., *ACS Applied Materials & Interfaces* **2021,** *13* (48), 57067-57074.
(31) Lv, Y.; Cui, L.; Peng, R.; Zhao, Z.; Qiu, L.; Chen, H.; Jin, C.; Zhang, X. B.; Tan, W., *Anal Chem* **2015,** *87* (23), 11714-20.
(32) He, L.; Lu, D.; Liang, H.; Xie, S.; Zhang, X.; Liu, Q.; Yuan, Q.; Tan, W., *Journal of the American Chemical Society* **2018,** *140* (1), 258-263.
(33) Meng, H. M.; Shi, X.; Chen, J.; Gao, Y.; Qu, L.; Zhang, K.; Zhang, X. B.; Li, Z., *ACS Sens* **2020,** *5* (1), 103-109.
(34) Li, J.; Weng, X.; Mo, F.; Han, M.; Li, H., *Anal Chem* **2020,** *92* (22), 15145-15151.
(35) Wu, T.; Cao, Y.; Zhang, Y.; Zheng, Z.; Li, J.; Li, H., *ACS Applied Nano Materials* **2022,** *5* (1), 537-545.
(36) Li, C.; Xue, C.; Wang, J.; Luo, M.; Shen, Z.; Wu, Z. S., *Anal Chem* **2019,** *91* (18), 11529-11536.
(37) Wang, D.-X.; Wang, J.; Wang, Y.-X.; Du, Y.-C.; Huang, Y.; Tang, A.-N.; Cui, Y.-X.; Kong, D.-M., *Chemical Science* **2021,** *12* (22), 7602-7622.
(38) Feng, Y.; Liu, Q.; Zhao, X.; Chen, M.; Sun, X.; Li, H.; Chen, X., *Anal Chem* **2022,** *94* (6), 2934-2941.
(39) Chai, S. Q.; Lv, W. Y.; He, J. H.; Li, Y. F.; Zou, H. Y.; Li, C. M.; Huang, C. Z., *Anal Chem* **2021,** *93* (43), 14545-14551.
(40) Zhang, J.; Fu, H.; Chu, X., *Anal Chem* **2021,** *93* (44), 14675-14684.
(41) Yang, H.; Liu, A.; Wei, M.; Liu, Y.; Lv, B.; Wei, W.; Zhang, Y.; Liu, S., *Analytical Chemistry* **2017,** *89* (22), 12094-12100.
(42) Xu, X.; Wang, L.; Li, K.; Huang, Q.; Jiang, W., *Analytical Chemistry* **2018,** *90* (5), 3521-3530.
(43) Ebrahimi, S. B.; Samanta, D.; Mirkin, C. A., *Journal of the American Chemical Society* **2020,** *142* (26), 11343-11356.
(44) Huang, Z.; Qiu, L.; Zhang, T.; Tan, W., *Matter* **2021,** *4* (2), 461-489.
(45) Lacroix, A.; Vengut-Climent, E.; de Rochambeau, D.; Sleiman, H. F., *ACS central science* **2019,** *5* (5), 882-891.
(46) Conde, J.; Oliva, N.; Atilano, M.; Song, H. S.; Artzi, N., *Nature Materials* **2016,** *15* (3), 353-363.
(47) Donati, B.; Ciarrocchi, A., *International Journal of Molecular Sciences* **2019,** *20* (12).
(48) Liu, A.-N.; Qu, H.-J.; Gong, W.-J.; Xiang, J.-Y.; Yang, M.-M.; Zhang, W., *Journal of Cellular Biochemistry* **2019,** *120* (9), 14860-14866.
(49) Li, L.; Ren, Y.; Wen, X.; Guo, Q.; Wang, J.; Li, S.; Yang, M.; Wang, K., *Anal Chem* **2021,** *93* (41), 13919-13927.
(50) Deng, W.; Chen, G.; Xiong, D.; He, R.; Wang, K.; Lu, H.; Kong, J., *Anti-Cancer Drugs* **2022,** *33* (9).

https://dspace.org/

Entropy-driven three-dimensional DNA nanofireworks for simultaneous real-time imaging of telomerase and microRNA in living cells

Wang, Jin; Wang, Kaixuan; Peng, Hanyong; Zhang, Zhen; Yang, Zhugen ...

2023-02-28
American Chemical Society
https://doi.org/10.1021/acs.analchem.2c05200
Wang J, Wang K, Peng H, et al., (2023) Entropy-driven three-dimensional DNA nanofireworks for simultaneous real-time imaging of telomerase and microRNA in living cells. Analytical Chemistry, Volume 95, Issue 8, February 2023, pp. 4138-4146

Downloaded from a DSpace repository. https://dspace.org/